Supplemental Materials (JCI130562DS1)

Specificity of bispecific T cell receptors and antibodies targeting peptide-HLA

Christopher J. Holland[*1], Rory M. Crean[*2,3], Johanne M. Pentier[*1], Ben de Wet[*1], Angharad Lloyd[1*], Velupillai Srikannathasan[1], Nikolai Lissin[1], Katy A. Lloyd[1], Thomas H. Blicher[1], Paul J. Conroy[1], Miriam Hock[1], Robert J. Pengelly[1], Thomas E. Spinner[1], Brian Cameron[1], Elizabeth A. Potter[1], Anitha Jeyanthan[1], Peter E. Molloy[1], Malkit Sami[1], Milos Aleksic[1], Nathaniel Liddy[1], Ross A. Robinson[1], Stephen Harper[1], Marco Lepore[1], Chris R. Pudney[2], Marc W. van der Kamp[4], Pierre J. Rizkallah[5], Bent K. Jakobsen[1], Annelise Vuidepot[1] and David K. Cole[1]

[1]Immunocore Ltd., Milton Park, Abingdon, UK.
[2]Department of Biology and Biochemistry, University of Bath, Bath, UK.
[3]Doctoral Training Centre in Sustainable Chemical Technologies, University of Bath, Bath, UK.
[4]School of Biochemistry, University of Bristol, Biomedical Sciences Building, University Walk, Bristol, UK.
[5]Cardiff University School of Medicine, Heath Park, Cardiff, UK.
[*]These authors contributed equally to this study.

Supplemental Methods

Analysis of on-target and off-target T cell reactivity via re-direction using anti-pHLA/anti-CD3 bispecific reagents

The activity of the ImmTAC molecules (TCR-CD3 scFv fusions) and the TCR-mimic scFv-CD3 scFv fusions was tested through their ability to redirect T cells against a range of antigen-positive and antigen-negative cell lines (tumour and healthy cells). Incucyte killing assays were performed according to the manufacturer's instructions (Sartorius, UK). Briefly, 100,000 PBMCs per well were added to 10,000 target cells per well. Target cells included HLA-A*02:01 and HLA-A*01:01 positive tumour cell lines, which were positive or negative for expression of target protein, as well as a panel of healthy cell lines. Target cells were incubated on plates overnight at 37°C in 5% CO^2 before addition of ImmTAC molecules, or TCR-mimic bispecific reagents at 10^{-7} – 10^{-12} M followed by PBMCs and CellPlayer kinetic caspase apoptosis assay kit™. Cells were scanned every 3 hours for 70 hours, and data were quantified using IncuCyte ZOOM software™ (Sartorius, UK). Results were analysed using GraphPad Prism. For IFNγ ELISPOT assay, experiments were performed according to the manufacturer's instructions (BD BioSciences, UK). Briefly, 80,000 PBMCs per well were added to 50,000 target cells per well. Target cells included HLA-A*0201 positive tumour cell lines, positive or negative for expression of target protein, as well as a panel of healthy cell lines. ImmTAC molecules, or TCR-mimic bi-specific reagents were added at 10^{-7} – 10^{-12} M and incubated overnight at 37°C in 5% CO2. Data were quantified after development using an automated ELIspot reader (ImmunoSpot Series 5 analyser, Cellular Technology Ltd.). For multiplex cytokine analysis $CD4^+$ and $CD8^+$ T cells from a healthy donor were isolated by magnetic separation using negative selection kits following manufacturer's instructions (Miltenyi, Germany). T cells were cultured with target cell lines at an E:T ratio of 5:1 with 10nM, 100pM or 1pM of either ImmTAC or TCR-mimic bispecific for 48hrs. Cell supernatants were collected and tested using a Human TH1/TH2 10-Plex Tissue Culture Kit following the manufactures instructions and analysed on a MESO QuickPlex SQ 120 (MSD, USA).

Construct design, protein expression and purification

The HLA-A*01:01 and HLA-A*02:01 heavy chains were expressed with a biotinylation tag (for SPR experiments), or without it (for crystallisation screens) and refolded in the presence of β2m and a specific peptide, as previously described (1). TCRs and scFv were both refolded and purified using a previously described TCR refolding protocol (2). For a 250 ml ImmTAC molecule refold, 6.5 mg α-chain was mixed with 16 mg β-chain. The refolds were extensively dialysed against 20 mM Tris pH8 at 8°C and purified by Poros50HQ™ 10/100, Poros50HS™ 10/100 (Life Technologies) and Superdex S200HR™ 10/300 (GEH) columns (3).

SPR Single cycle kinetic analysis

pHLAs were biotinylated as described previously (4) and were immobilised onto a streptavidin-coupled CM5 sensor chip. For alanine scan analysis, 500 RUs of each alanine scan mutant were loaded onto individual flow cells. Flow cell one was loaded with free biotin to act as a control surface. All measurements were performed at 25°C in PBS buffer (Sigma, UK) at a flow rate of 30 µl/min. Binding profiles of the TCRs and TCR-mimic antibodies were determined using single cycle kinetic analysis as previously reported (5, 6). TCRs and TCR-mimic antibodies were injected at a top concentration of around 20 µM, followed by four injections using serial 1/3 dilutions. K_D values were calculated assuming Langmuir binding (AB = B*AB_{max} / (KD + B)) and data were analysed using the kinetic titration algorithm (BIAevaluationTM 3.1) (7).

Generation of scHLA libraries

scHLAs were displayed on the surface of phage with the peptide component disulphide trapped in a single chain trimer (dsSCT). Diversity was encoded at the peptide level by introducing a flat distribution of 19 amino acids (excluding cysteine, to avoid cyclic peptide formation). All 19 amino acids were represented at the HLA primary anchors, Pos2 and Pos9, however, to maximise the functionality of the library with peptide correctly bound in the antigen binding groove, the amino acid distribution was biased towards to known anchor residue preferences for HLA-A*02:01. This phagemid library was introduced by electroporation into E. coli TG1 cells and grown in 2xYT amp 2% glucose media to OD600 = 0.5 and HelperPhage added at an infection ratio of ~ 20:1 phage to E. coli. Phage particles were isolated by PEG precipitation and 0.45 µM filtration. Panning was performed using 200nM for pan 1, and then decreasing concentrations (0.048 nM – 94nM) in subsequent pans to increase selection pressure.

pHLA libraries preparation

A primer containing molecular index was annealed to a region upstream of the peptide sequence on the scHLA-pIM627 phagemid DNA and single primer extension reaction was carried out with Kapa HiFi DNA polymerase (Roche Diagonostics). Following a reaction cleanup with ExoProStar (GE Healthcare) and column purification (Macherey-Nagel), second PCR reaction was carried out with primers specific to the primer containing molecular index and a reverse primer designed to the β2M gene. Sequencing libraries were prepared from purified PCR products (Ampure XP beads, Beckman coulter) using NebNext Ultra II DNA library prep kit (NEB) according to manufacturer's instructions. Library QC was performed with Agilent bioanalyser HS kit (Agilent biosystems) and library DNA concentrations were measured with Qubit HS dsDNA kit (Life technologies). Libraries were sequenced using Illumina V3 SBS chemistry on the MiSeq sequencer. Basecalling and sample demulitplexing was performed using MiSeq reporter to generate fastq files and were processed with custom analysis pipeline. Peptide repertoire analysis was performed using excel and sequence Logos were generated using IceLogo standalone tool (8). Sequence clustering analysis was performed with GibbsCluster-2.0 web server using default settings (9).

MD Simulations and MMPBSA calculations

Molecular Mechanics Poisson–Boltzmann Surface Area (MMPBSA) calculations were performed using MMPBSA.py.MPI (10), using 25 independent (random velocity vectors assigned upon heating) 4 ns long MD simulations (see section "Structure equilibration procedure") for each structure. From each run, 300 equally spaced snapshots were taken from the last 3 ns of each MD simulation for MMPBSA calculations, giving a total of 7500 frames per complex. MMPBSA calculations were performed with an implicit salt concentration of 150 mM, and with 30 explicit water molecules (which were all defined as part of the receptor) retained in each snapshot. The 30 closest water molecules to any binding site residue heavy atom were retained in each snapshot by using the 'closest' command in CPPTRAJ (11), (see section "Selection of explicit waters for MMPBSA calculations" for further details).

Structure equilibration procedure

The following procedure was used to prepare for production MD simulations for both the long time-scale (2 x 500 ns) and short time scale (25 x 4 ns) simulations used in this study. First, hydrogen atoms and solvent molecules were relaxed with 500 steps of steepest descent followed by 500 steps of conjugate gradient (using 10 kcal mol^{-1} $Å^{-1}$ positional restraints on all protein heavy atoms). The system was then heated linearly from 50 K to 298 K (NVT ensemble) over the course of 200 ps (retaining the 10 kcal mol^{-1} $Å^{-1}$ positional restraints on all protein heavy atoms). The whole system was then minimised for a further 500 steps of steepest descent followed by 500 steps of conjugate gradient with 5 kcal mol^{-1} $Å^{-1}$ positional restraints on all Cα carbon atoms. Retaining the Cα carbon restraints, each system was again heated from 25 K to 298 K over the course of 50 ps in the NVT ensemble. The Cα carbon restraints were then gently removed in linear steps of (5, 4, 3, 2, 1, 0 kcal mol^{-1} $Å^{-1}$) of 10 ps each in the NPT ensemble. Following this, production MD simulations were run. For NVT simulations, the timestep was set to 1 fs (with the SHAKE algorithm applied) and a collision frequency of 1 ps^{-1} was used with Langevin temperature control. Simulations in the NPT ensemble were performed with a timestep of 2 fs (with the SHAKE algorithm applied), using a Berendsen barostat for pressure control (1 ps pressure relaxation time) and Langevin temperature control (collision frequency of 1 ps^{-1}).

Selection of explicit waters for MMPBSA calculations

The InterfaceResidues.py script (available at https://pymolwiki.org/index.php/InterfaceResidues) run through PyMOL on each crystal structure was used to identify in an unbiased manner the binding site residues for each TCR/Fab-pHLA. Criteria for selecting interfacial residues were set based on the results of Maffucci et al. (12) (Cut-off for change in solvent accessible surface area was set to 0.5 $Å^2$ for all residues). Following this, CPPTRAJ (11) (part of the AmberTools suite of programmes), was used to select the closest 30 water molecules to the selected interfacial residues using the 'closest' command. Stripping solvent using large residue selections such as the ones generated in these calculations can be time consuming if performed on the entire water box. To greatly increase the speed of this calculation, we performed two 'closest' calculations (one to remove most of the waters in the periodic box, and the second to select the 30 closest waters molecules for MMPBSA calculations). An example script of how to do this within CPPTRAJ is shown below:

Example closest waters calculation command

```
------------------------------------------------------ START OF SCRIPT ----------------------------------------
 # Run with command cpptraj -i [Script_Input] > [Termimal_Output]
parm [TopologyFile]
trajin [TrajectoryFile]
strip :Na+,Cl- # remove any salt from trajectory
autoimage # image once now instead of two imaging steps later (for each closest command)
solvent byres :WAT
# Run closest command on large number of waters…
# picking only a single (or very few) atom(s).
closest 2000 [residue/atom selection] center noimage
# You should visualise the output of this command before continuing…
# to ensure enough water surrounds your binding site for the subsequent calculation.
# In next step, save the topology.
# This can be used as the complex topology file for MMPB/GBSA calculations
closest 30 [residuemask] noimage outprefix [PrefixName]
trajout [TrajectoryOutFile]
run
exit
------------------------------------------------------ END OF SCRIPT ----------------------------------------
```

References for Supplemental Methods

1. Bulek AM et al. Structural basis for the killing of human beta cells by CD8(+) T cells in type 1 diabetes. *Nat. Immunol.* 2012;13(3):283–289.
2. Boulter JM et al. Stable, soluble T-cell receptor molecules for crystallization and therapeutics. *Protein Eng.* 2003;16(9):707–11.
3. Liddy N et al. Monoclonal TCR-redirected tumor cell killing. *Nat. Med.* 2012;18(6):980–7.
4. Cole DK et al. Computational design and crystal structure of an enhanced affinity mutant human CD8 alphaalpha coreceptor. *Proteins* 2007;67(1):65–74.
5. Madura F et al. T-cell receptor specificity maintained by altered thermodynamics. *J. Biol. Chem.* 2013;288(26):18766–75.
6. Cole DK et al. T-cell Receptor (TCR)-Peptide Specificity Overrides Affinity-enhancing TCR-Major Histocompatibility Complex Interactions *J. Biol. Chem.* 2014;289(2):628–638.
7. Karlsson R, Katsamba PS, Nordin H, Pol E, Myszka DG. Analyzing a kinetic titration series using affinity biosensors *Anal. Biochem.* 2006;349(1):136–147.
8. Colaert N, Helsens K, Martens L, Vandekerckhove J, Gevaert K. Improved visualization of protein consensus sequences by iceLogo *Nat. Methods* 2009;6(11):786–787.
9. Andreatta M, Lund O, Nielsen M. Simultaneous alignment and clustering of peptide data using a Gibbs sampling approach *Bioinformatics* 2013;29(1):8–14.
10. Miller BR et al. *MMPBSA.py* : An Efficient Program for End-State Free Energy Calculations *J. Chem. Theory Comput.* 2012;8(9):3314–3321.
11. Roe DR, Cheatham TE. PTRAJ and CPPTRAJ: Software for Processing and Analysis of Molecular Dynamics Trajectory Data *J. Chem. Theory Comput.* 2013;9(7):3084–3095.
12. Maffucci I, Contini A. Improved Computation of Protein–Protein Relative Binding Energies with the Nwat-MMGBSA Method *J. Chem. Inf. Model.* 2016;56(9):1692–1704.

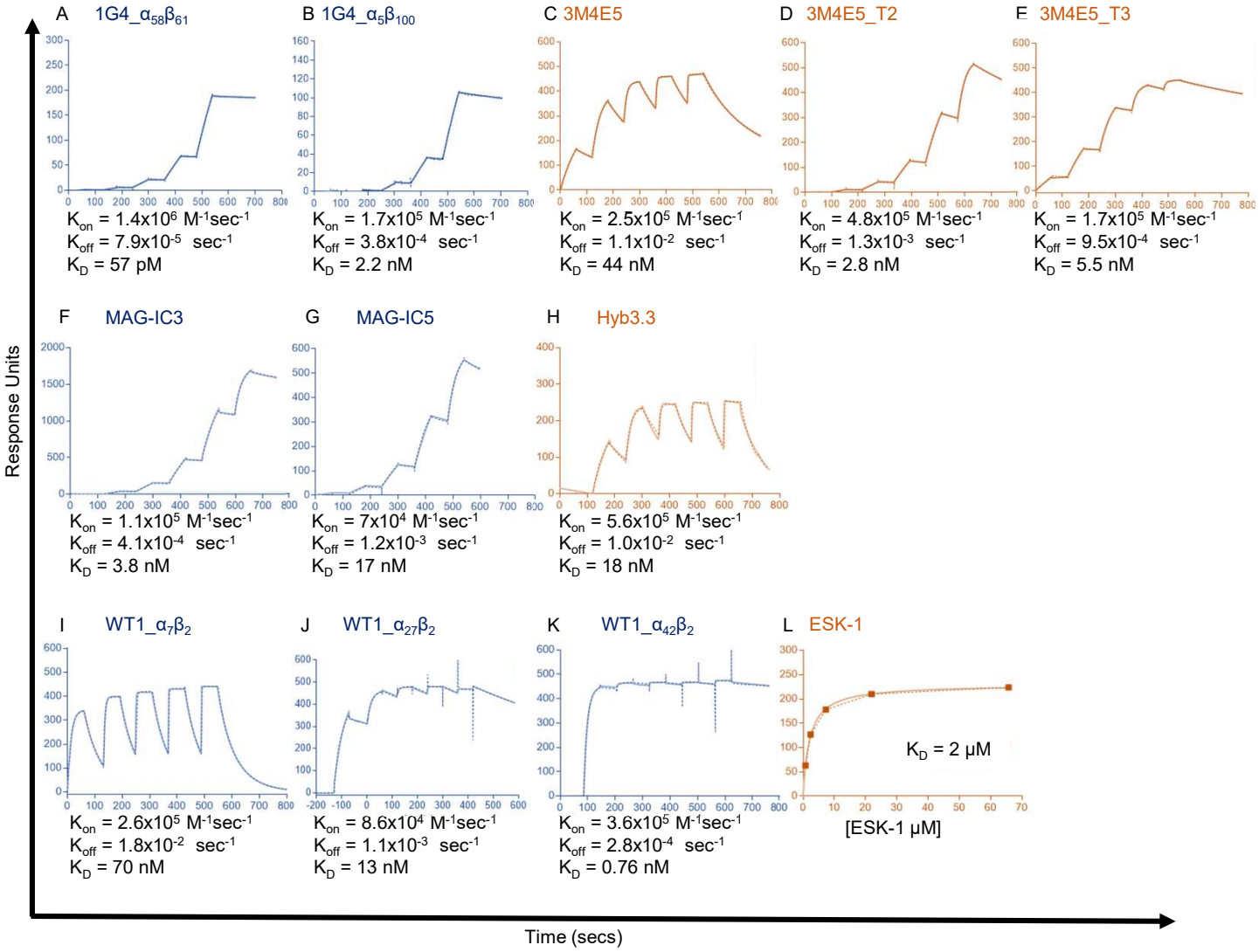

Supplemental Figure 1: – Binding affinity analysis of affinity-enhanced TCRs and TCR-mimics
The interaction between each affinity-enhanced TCR, or TCR-mimic with cognate pHLA molecules was analysed using surface plasmon resonance. Binding affinities of the affinity-enhanced TCRs and TCR-mimics were determined using single cycle kinetic analysis, or equilibrium binding analysis (for ESK-1). Five injections of each reagent were performed using 3:1 dilution between injections. Raw data (dotted line) and fits (solid line) are shown for each plot. Representative data from three independent experiments are shown. **A-B**) A2-SLL affinity-enhanced TCRs (1G4_$\alpha_{58}\beta_{61}$ and 1G4_$\alpha_5\beta_{100}$), **C-E**) A2-SLL TCR-mimics (3M4E5, 3M4E5_T2 and 3M4E5_T3), **F-G**) A1-EVD affinity-enhanced TCRs (MAG-IC3 and MAG-IC5), **H**) Hyb3-A1-EAD, **I-K**) A2-RMF affinity-enhanced TCRs (WT1_$\alpha_7\beta_2$, WT1_$\alpha_{27}\beta_2$ and WT1_$\alpha_{42}\beta_2$), **L**) ESK-1-A2-RMF.

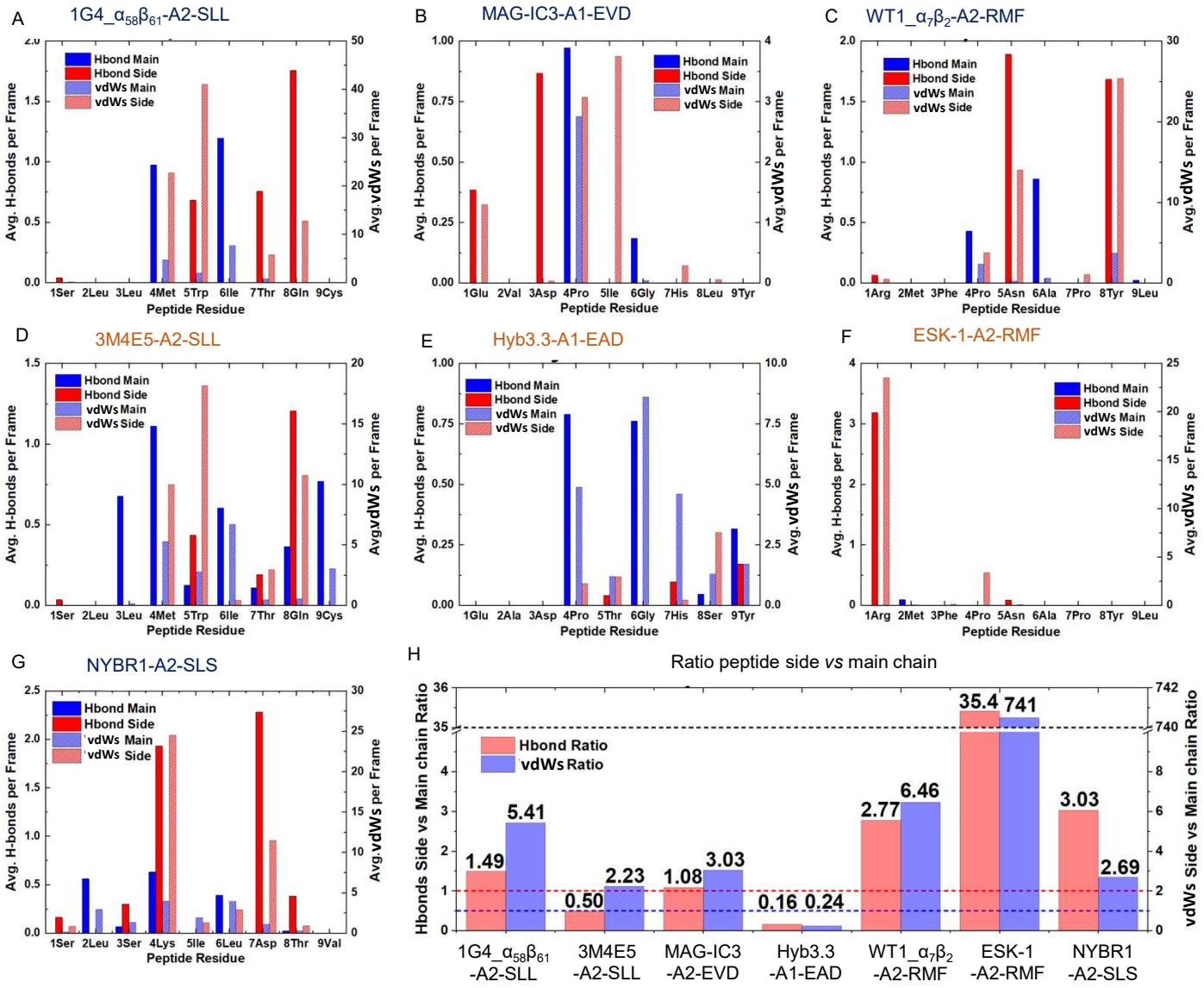

Supplemental Figure 2: – Molecular dynamic analysis of the TCR and TCR-mimic-peptide interface
Molecular dynamics was performed to access the average number of side chain or main chain peptide contacts over time. MD simulations were performed using 2 independent (random velocity vectors assigned upon heating) 500 ns long MD simulations for each structure. Average number of hydrogen bonds and vdWs interactions formed per frame between the peptide and the TCR/Fab over the course of our long time scale MD simulations. Per-residue peptide contributions are divided into main (blue and light blue) and side (red and light red) chain contributions. **A)** 1G4_$\alpha_{58}\beta_{61}$-A2-SLL, **B)** MAG-IC3-A1-EVD, **C)** WT1_$\alpha_7\beta_2$-A2-RMF, **D)** 3M4E5-A2-SLL, **E)** Hyb3.3-A1-EAD, **F)** ESK-1-A2-RMF. **G**) NYBR1 TCR, **H**) Ratio of total peptide side chain against peptide main chain hydrogen bonds (red) and vdWs interactions (blue) for each TCR/Fab-pHLA. Ratios are stated above each bar to 3 significant figures. The red and blue dotted lines represent the y-axis location for a ratio of 1 for Hydrogen bonds and vdWs interactions respectively. A black dotted line denotes the position of an axis break used to allow ESK-1 Fab to be plotted on the same graph.

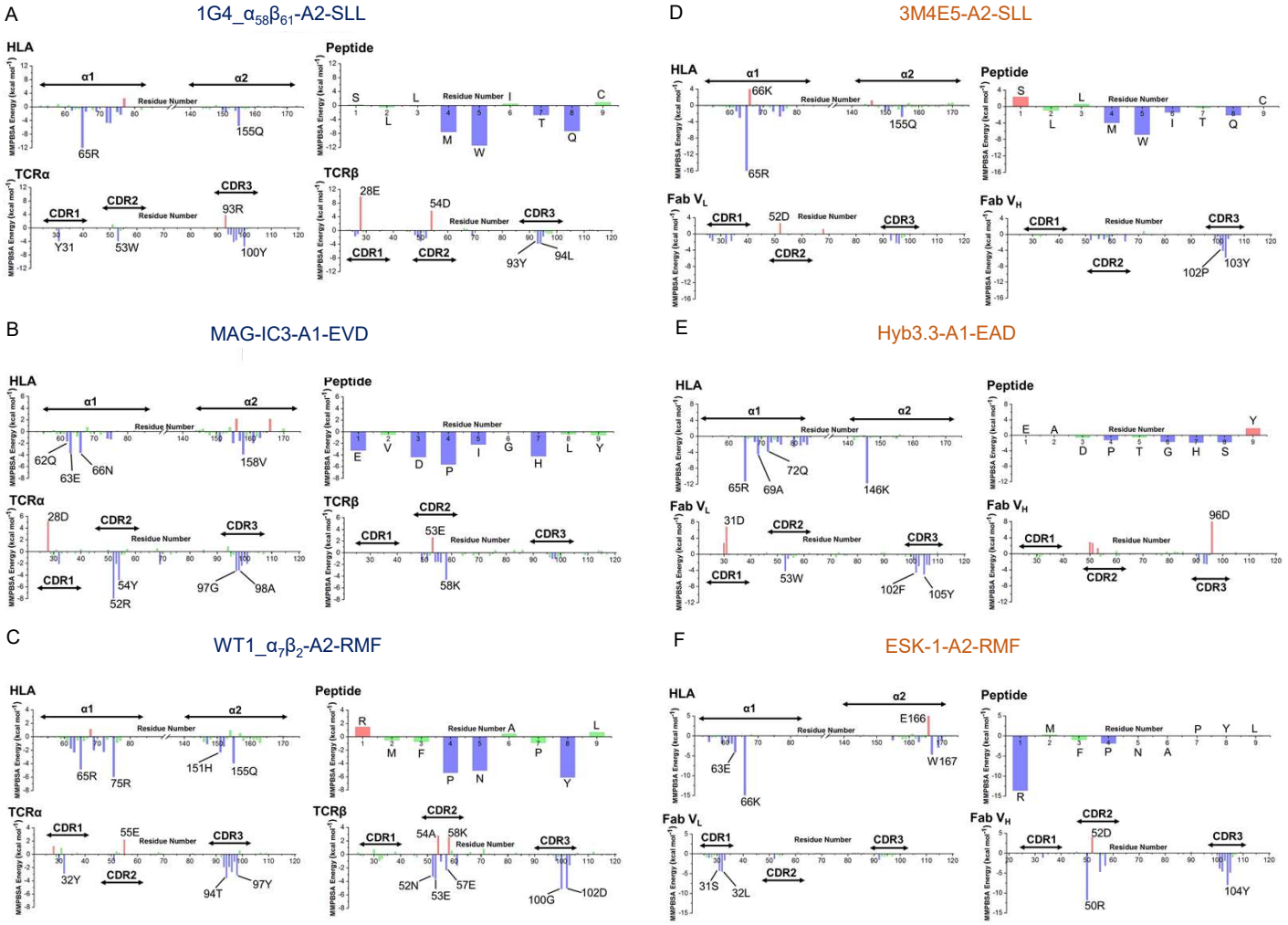

Supplemental Figure 3: Per-residue decomposition of the binding free energy obtained from MMPBSA calculations for key regions of **A)** 1G4_$\alpha_{58}\beta_{61}$-A2-SLL, **B)** MAG-IC3-A1-EVD, **C)** WT1_$\alpha_7\beta_2$-A2-RMF, **D)** 3M4E5-A2-SLL, **E)** Hyb3.3-A1-EAD, **F)** ESK-1-A2-RMF. A more negative value indicates increased favourability towards binding. Bars are coloured as follows: blue, less than -1 kcal mol^{-1}; green, between -1 and 1 kcal mol^{-1}; and red, greater than 1 kcal mol^{-1}. MD simulations were performed using 25 independent (random velocity vectors assigned upon heating) 4 ns long MD simulations for each structure.

A

Average Transcripts/ 100ng RNA

Cell line name	COLO 205	HCC 1428	HEP-G2	NCI-H1703	NCI-H1755	NCI-H1944	NCI-H2087	NCI-H441	HlSMC	Ren8
Tissue	Colon	Breast	Liver	Lung	Lung	Lung	Lung	Lung	Intestine	Kidney
NYESO-1	0	6,522	0	132,103	284,394	256	0	4	0	0
MAGE-A3	3	62,648	27	77,279	112,693	2,860	12	0	0	0
MAGE-A1	17	288,126	47	423,610	2,279	4,531	15	5	23	0

B

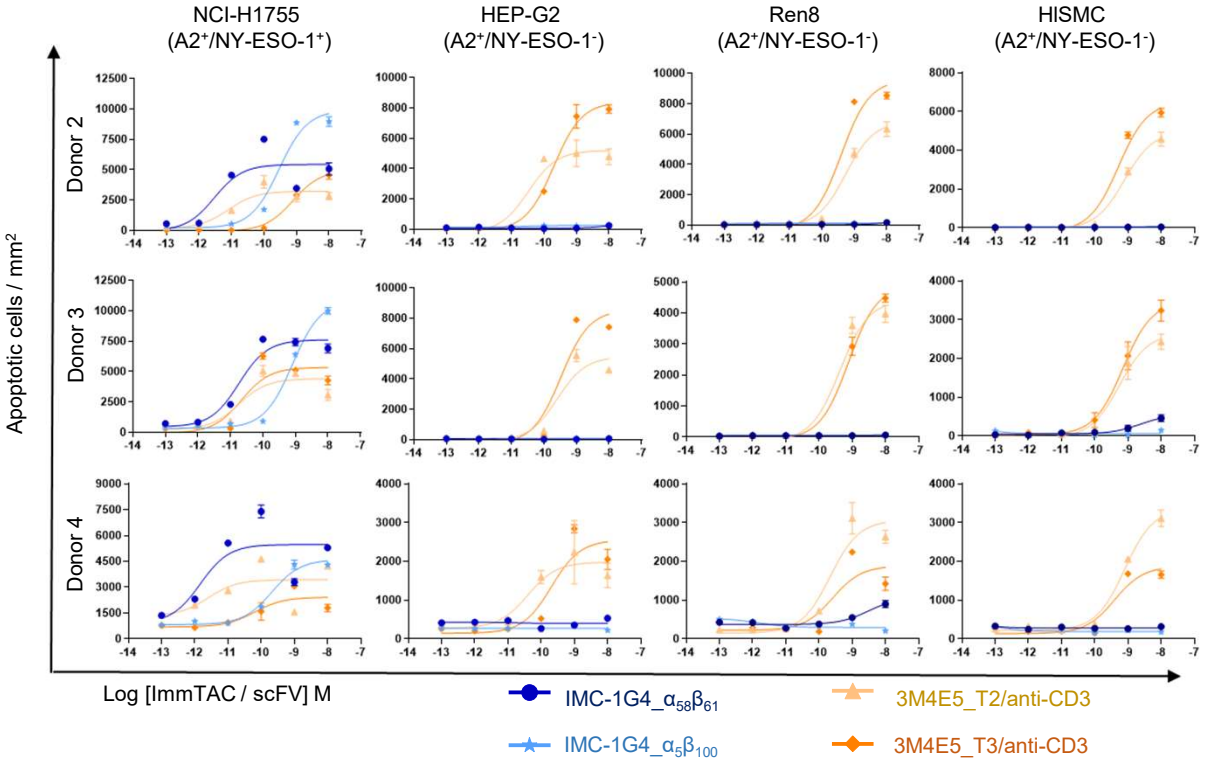

C

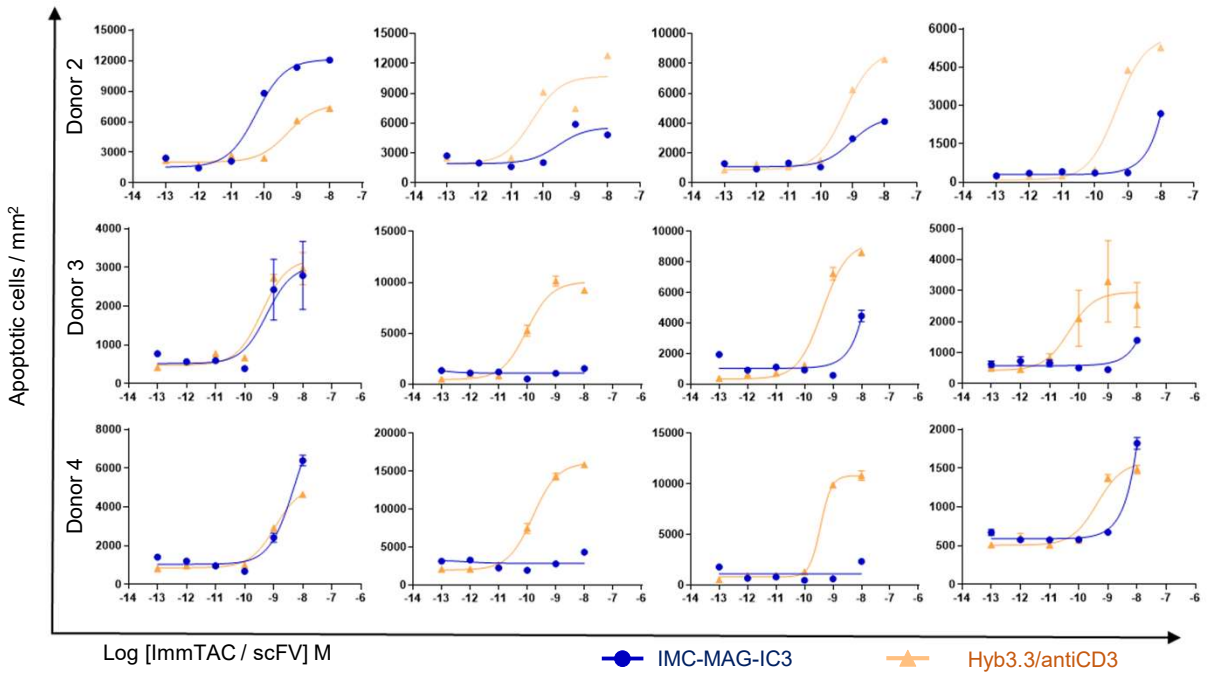

Supplemental Figure 4: – **A)** Antigen expression of each cell line was tested by analysing the mRNA transcript levels (at least n=3 for each gene tested). Average transcript number per 100ng of RNA detailed in the table. **B-C)** The activity of the ImmTAC molecules and the TCR-mimic-anti-CD3 fusions was tested against a range of antigen positive and antigen negative cell lines (tumour and healthy cells) using IncuCyte killing assays in 3 further donors. Data are plotted using area under the curve analysis. Error bars show standard deviation from three experimental repeats. **B)** IMC-1G4_$\alpha_{58}\beta_{61}$, 3M4E5_T2/anti-CD3 and 3M4E5_T3/anti-CD3 T cell re-direction against HLA-A*02:01^{+}/NY-ESO-1^{+} (NCI-H1755) and HLA-A*02:01^{+}/NY-ESO-1^{-} (HEP-G2, Ren8 and HISMC) cells lines. **C)** IMC-MAG-IC3 and Hyb3.3/anti-CD3 T cell re-direction against HLA-A*01:01^{+}/MAGE-A3^{+} (HCC1428 and NCI-H1703), HLA-A*01:01^{+}/MAGEA1^{+} (HCC1428 and NCI-H1703) and HLA-A*01:01^{+}/MAGE^{-} (COLO205 and HISMC) cells lines.

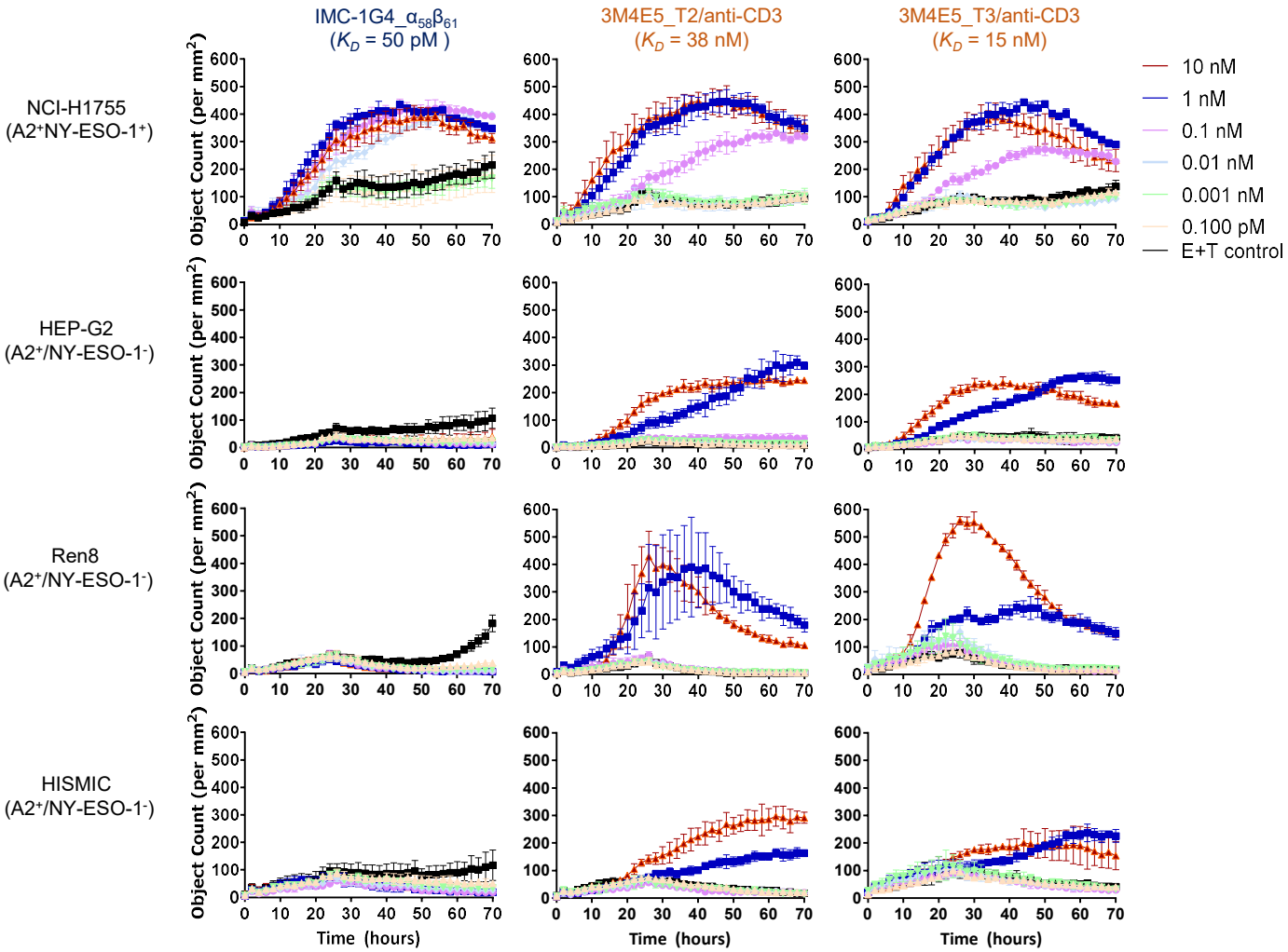

Supplemental Figure 5: The activity of IMC-1G4_$\alpha_{58}\beta_{61}$, 3M4E5_T2/anti-CD3 and 3M4E5_T3/anti-CD3 was tested against against HLA-A*02:01^{+}/NY-ESO-1^{+} (NCI-H1755) and HLA-A*02:01^{+}/NY-ESO-1^{-} (HEP-G2, Ren8 and HISMC) cells lines using Incucyte killing assays. Experiments were performed according to the manufacturer's instructions (Sartorius, UK). 100,000 PBMCs per well were added to 10,000 target cells per well. Target cells were incubated on plates overnight before addition of ImmTAC molecules, or TCR-mimic bispecific reagents followed by PBMCs. Cells were scanned every 3 hours for 70 hours. Data are plotted using cell death over time. Data from 1 out of 2 donors shown. Error bars show standard deviation from three experimental repeats.

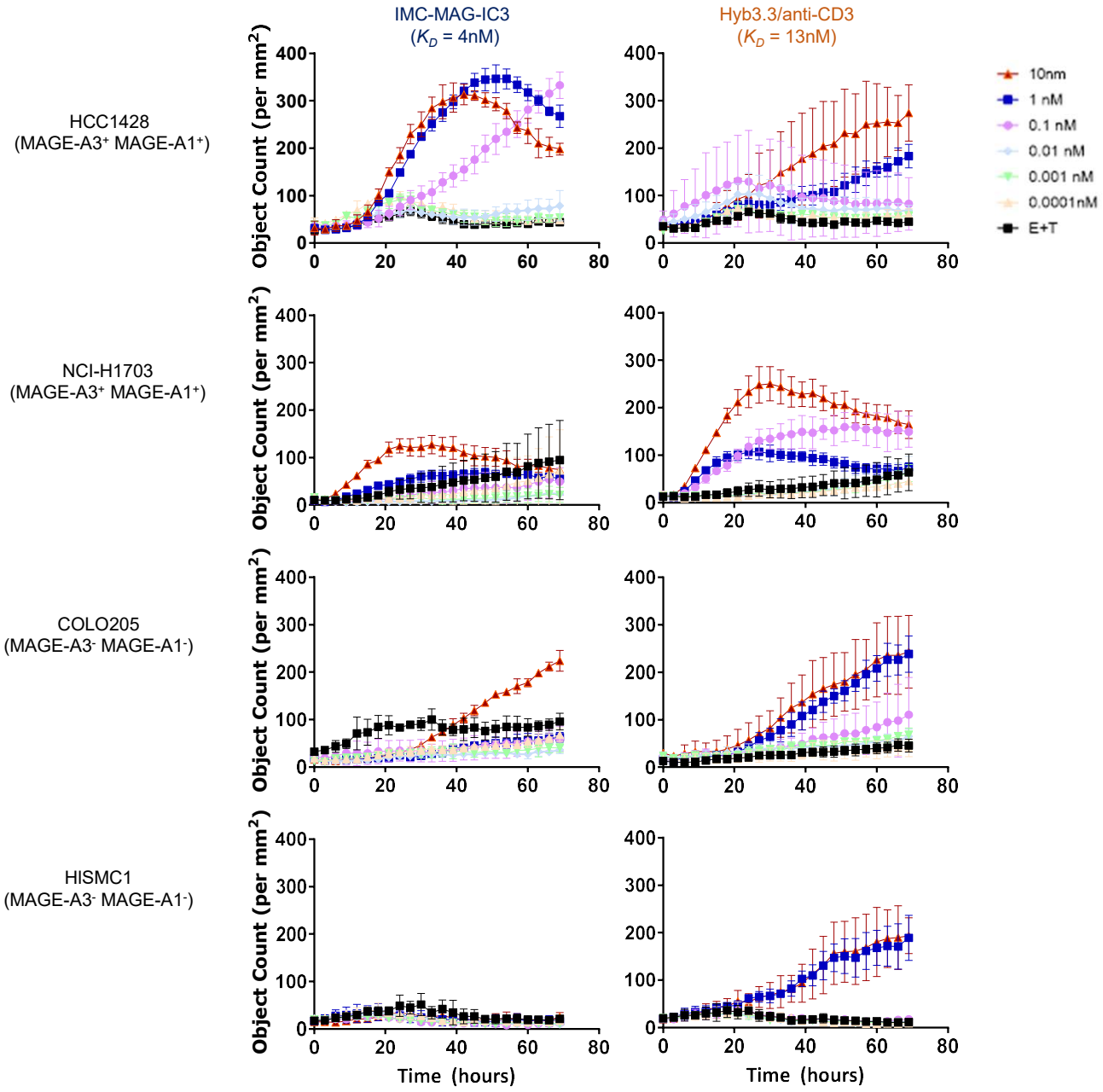

Supplemental Figure 6: The activity of IMC-MAG-IC3 and Hyb3.3/anti-CD3 was tested against HLA-A*01:01$^+$/MAGE-A3$^+$ (HCC1428 and NCI-H1703), HLA-A*01:01$^+$/MAGE-A1$^+$ (HCC1428 and NCI-H1703) and HLA-A*01:01$^+$/MAGE$^-$ (COLO205 and HISMC) cells lines using Incucyte killing assays. Experiments were performed according to the manufacturer's instructions (Sartorius, UK). 100,000 PBMCs per well were added to 10,000 target cells per well. Target cells were incubated on plates overnight before addition of ImmTAC molecules, or TCR-mimic bispecific reagents followed by PBMCs. Cells were scanned every 3 hours for 70 hours. Data are plotted using cell death over time. Data from 1 out of 2 donors shown. Error bars show standard deviation from three experimental repeats.

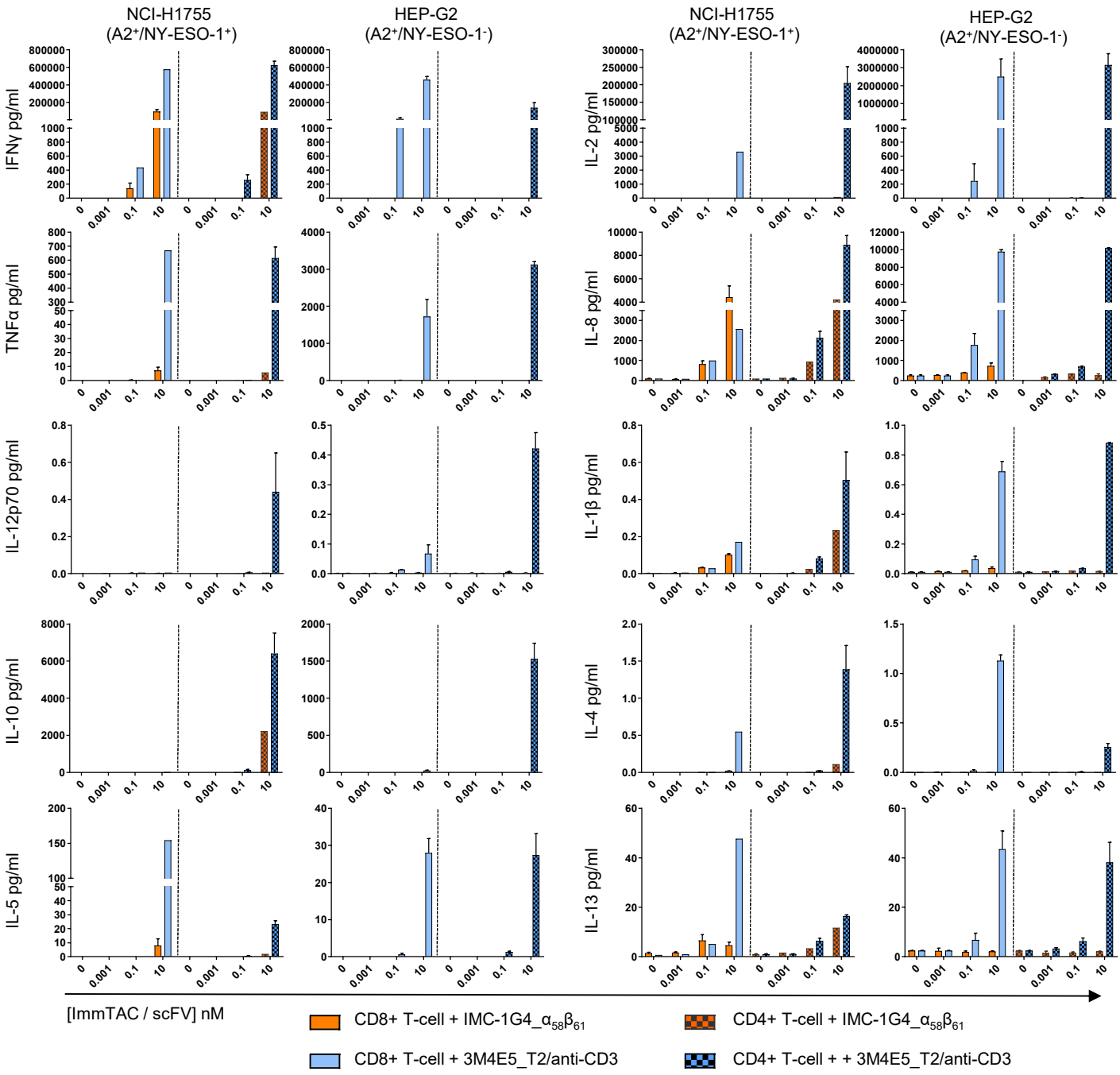

Supplemental Figure 7: Cytokine profiles of isolated CD8$^+$ or CD4$^+$ T cells generated upon redirection by either IMC-1G4_$\alpha_{58}\beta_{61}$ or 3M4E5_T2/anti-CD3 against NCIH-1755 (HLA-A*02:01$^+$/NY-ESO-1$^+$) or HEP-G2 (HLA-A*02:01$^+$/NY-ESO-1$^-$). CD8$^+$ and CD4$^+$ T cell populations were isolated by magnetic separation *via* negative selection to a purity of ≥85% and cultured with target cells at an E:T ratio of 5:1 with either 10nM, 100pM or 1pM of IMC-1G4_α58β61 or 3M4E5_T2-anti-CD3 for 48hrs. Cell supernatants were collected and a cytokine multiplex analysis for IFNγ, IL-2, TNFα, IL-8, IL-12p70, IL-1β, IL-10, IL-4, IL-5 and IL-13 was performed. Error bars show standard deviation from three experimental repeats.

A

NYBR1-A2-SLSKILDTV

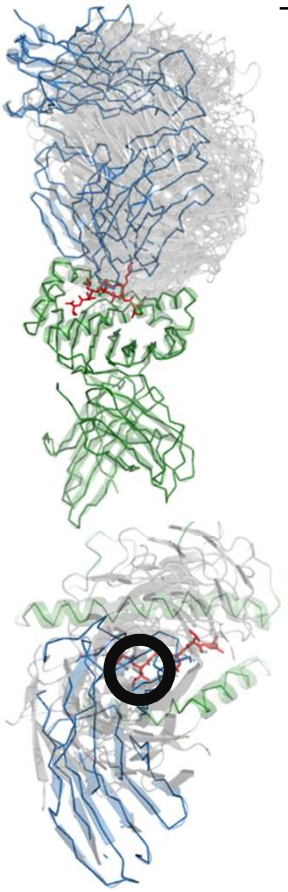

	NYBR1 TCR
Affinity (K_D)	47pM
PDB	6R2L
Crossing angle °	63.6
Total Bonds	149
Pep bonds (bold >10)	2, 3, **4**, 5, 6, 7, 8
MHC >5 bonds (bold >10)	62, **65**, 73, **154**, **155**, 157, 163, 166
MHC bonds	102
Pep bonds	47 (32%)
BSA total Å²	2835
BSA α/H Pep Å²	311
BSA β/L Pep Å²	450
BSA α/H MHC Å²	1412
BSA β/L MHC Å²	662

B

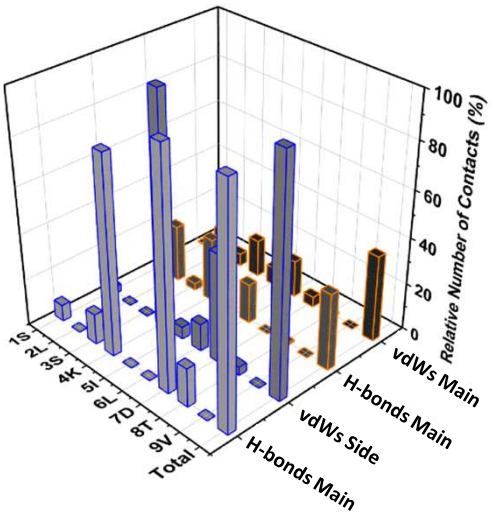

C

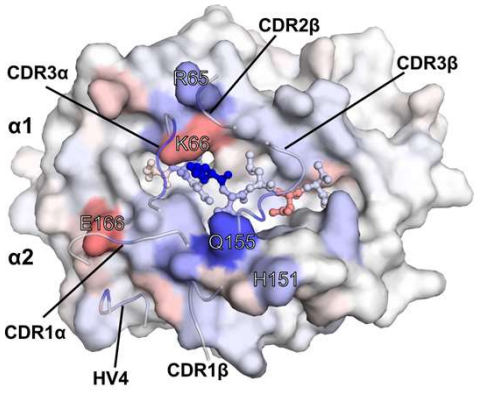

D

NYBR1-A2-SLS

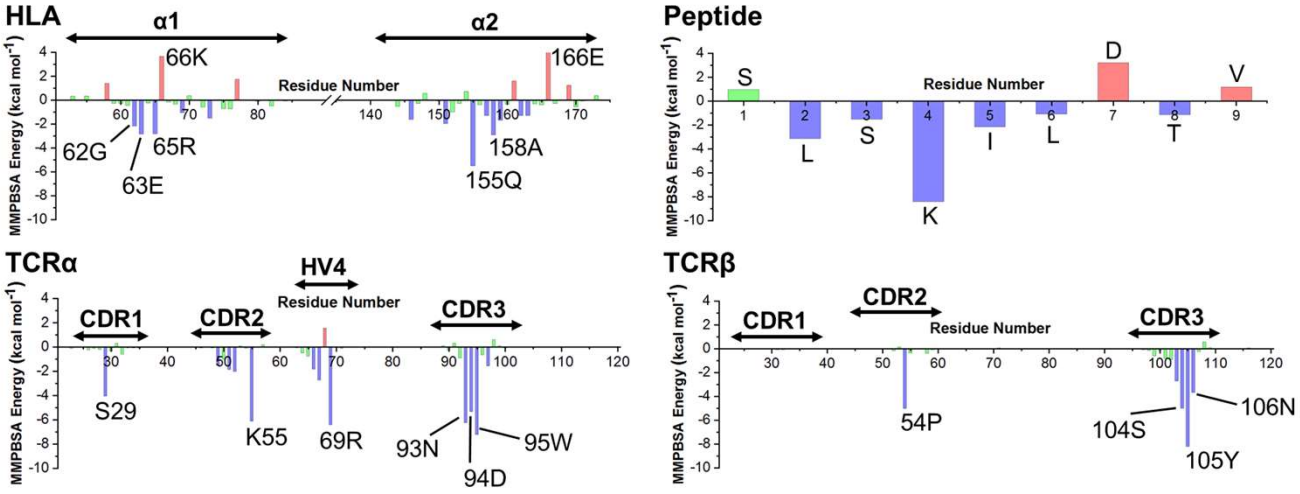

Supplemental Figure 8: A) Above: Side on view of the structure of the NYBR1 TCR (blue ribbon) in complex with A2 (green ribbon) -SLS (red sticks). Below: Top down view of the NYBR1 TCR-A2-SLS interaction. Black circles represent the center of binding. The table shows a structural analysis of the NYBR1-A2-SLS complex. Bonds were assessed using the program contact (CCP4), implementing a 3.4Å cut-off for Hydrogen bonds (H-bonds) and a 4Å cut-off for van der Waals (vdWs) interactions. Buried surface area (BSA) Å2 was determined using ePISA. **B)** Relative number of H-bonds and vdWs interactions formed between either the main or side chain of each peptide residue to the NYBR1 TCR over the course of our MD simulations. Total side versus main chain ratios for H-bonds and vdWs interactions are shown, with the larger value (side or main for each category) scaled to 100 % (absolute values for all contacts are provided in **Supplemental Figure 2**). MD simulations were performed using 25 independent (random velocity vectors assigned upon heating) 4 ns long MD simulations for each structure. **C)** Per-residue decomposition of the binding free energy obtained from our MMPBSA calculations, (as performed in Figure 5) to identify energetic hotspots in the NYBR1 TCR-A2-SLS interaction. A top down view of the pHLA is shown, with the peptide depicted as sticks and the HLA as a surface. Colour mapping of the decomposition results for each residue was performed across the entire binding interface and used to indicate which residues across this interface favour (blue) or disfavour (red) binding (with white indicating no preference). **D)** Per-residue decomposition of the binding free energy obtained from MM-PBSA calculations for key regions of NYBR1-A2-SLS. A more negative value indicates increased favourability towards binding. Bars are coloured as follows: blue, less than -1 kcal mol^{-1}; green, between -1 and 1 kcal mol^{-1}; and red, greater than 1 kcal mol^{-1}. MD simulations were performed using 25 independent (random velocity vectors assigned upon heating) 4 ns long MD simulations for each structure.

TCR-mimic	Target/peptide	HLA-A*	In vivo data	Structure	Refs
3M4E5	NY-ESO-1/SLIMWITQC	02:01	3M4E5_T2	3M4E5	(1–3)
ESK-1	WT1/RMFPNAPYL	02:01	ESK-1	ESK-1	(4–6)
Hyb3.3, G8	MAGE-A1/EADPTGHSY	01:01	Hyb3.3	Hyb3.3	(7–9)
PR20	PRAME/ALYVDSLFFL	02:01	PR20	No	(10)
38	LMP2A/CLGGLLTMV	02:01	38	No	(11)
G2D12	GP100/KTWGQYWQV	02:01	No	No	(12)
1A9, G1	GP100/IMDQVPFSV	02:01	No	No	(12)
2F1	GP100/YLEPGPVTA	02:01	No	No	(12)
GPA7	GP100/ITDQVPFSV	02:01	GPA7	No	(13)
4A9	hTERT/ILAKFLHWL	02:01	No	No	(14)
3H2	hTERT/RLVDDFLLV	02:01	No	No	(14)
M2B1	MUC1/LLLTVLTVV	02:01	No	No	(15)
7D4	MAGE-A3/FLWGPRALV	02:01	No	No	(16)
RL4B/3.2G1, 1B10	hCGβ/GVLPALPQV	02:01	RL4B/3.2G1	No	(17, 18)
3F9	hCGβ/TMTRVLQGV	02:01	No	No	(18)
1B8	Her2/ KIFGSLAFL	02:01	No	No	(19)
CAG10	MART-1/EAAGIGILTV	02:01	CAG10	No	(20)
Fab-D2	TARP/FLRNFSLML	02:01	No	No	(21)
T1-116C, T1-29D	p53/RMPEAAPPV	02:01	T1-116C	No	(22, 23)
T2-108A	p53/GLAPPQHLIRV	02:01	No	No	(24)
TA2	Tyrosinase/YMDGTMSQV	02:01	No	No	(25)
RL6A	p68/YLLPAIVHI	02:01	RL6A	No	(26)
RL21A	MIF/FLSELTQQL	02:01	RL21A	No	(27)
8F4	Proteinase 3/VLQELNVTV	02:01	No	No	(28)
#131	HA-1H/VLHDDLLEA	02:01	No	No	(29)

Supplemental Table 1. Summary of cancer-targeting TCR-mimic antibodies reported in the literature.

References for Supplemental Table 1

1. Stewart-Jones G et al. Rational development of high-affinity T-cell receptor-like antibodies *Proc. Natl. Acad. Sci.* 2009;106(14):5784–5788.
2. Held G et al. Dissecting cytotoxic T cell responses towards the NY-ESO-1 protein by peptide/MHC-specific antibody fragments. *Eur. J. Immunol.* 2004;34(10):2919–29.
3. Maus M V et al. An MHC-restricted antibody-based chimeric antigen receptor requires TCR-like affinity to maintain antigen specificity *Mol. Ther. - Oncolytics* 2016;3:16023.
4. Ataie N et al. Structure of a TCR-Mimic Antibody with Target Predicts Pharmacogenetics. *J. Mol. Biol.* 2016;428(1):194–205.
5. Dao T et al. Therapeutic bispecific T-cell engager antibody targeting the intracellular oncoprotein WT1 *Nat. Biotechnol.* 2015;33(10):1079–1086.
6. Dao T et al. Targeting the Intracellular WT1 Oncogene Product with a Therapeutic Human Antibody *Sci. Transl. Med.* 2013;5(176):176ra33-176ra33.
7. Chames P et al. TCR-like human antibodies expressed on human CTLs mediate antibody affinity-dependent cytolytic activity. *J. Immunol.* 2002;169(2):1110–8.
8. Chames P, Hufton SE, Coulie PG, Uchanska-Ziegler B, Hoogenboom HR. Direct selection of a human antibody fragment directed against the tumor T-cell epitope HLA-A1-MAGE-A1 from a nonimmunized phage-Fab library. *Proc. Natl. Acad. Sci. U. S. A.* 2000;97(14):7969–74.
9. Hülsmeyer M et al. A Major Histocompatibility Complex·Peptide-restricted Antibody and T Cell Receptor Molecules Recognize Their Target by Distinct Binding Modes *J. Biol. Chem.* 2005;280(4):2972–2980.
10. Chang AY et al. A therapeutic T cell receptor mimic antibody targets tumor-associated PRAME peptide/HLA-I antigens. *J. Clin. Invest.* 2017;127(7):2705–2718.
11. Ahmed M et al. TCR-mimic bispecific antibodies targeting LMP2A show potent activity against EBV malignancies. *JCI insight* 2018;3(4). doi:10.1172/jci.insight.97805
12. Denkberg G, Klechevsky E, Reiter Y. Modification of a tumor-derived peptide at an HLA-A2 anchor residue can alter the conformation of the MHC-peptide complex: probing with TCR-like recombinant antibodies. *J. Immunol.* 2002;169(8):4399–407.
13. Zhang G et al. Anti-melanoma activity of T cells redirected with a TCR-like chimeric antigen receptor. *Sci. Rep.* 2014;4(1):3571.
14. Lev A et al. Isolation and characterization of human recombinant antibodies endowed with the antigen-specific, major histocompatibility complex-restricted specificity of T cells directed toward the widely expressed tumor T-cell epitopes of the telomerase catalytic sub *Cancer Res.* 2002;62(11):3184–94.
15. Cohen CJ et al. Direct detection and quantitation of a distinct T-cell epitope derived from tumor-specific epithelial cell-associated mucin using human recombinant antibodies endowed with the antigen-specific, major histocompatibility complex-restricted specificity of T cells. *Cancer Res.* 2002;62(20):5835–44.
16. Bernardeau K et al. Assessment of CD8 involvement in T cell clone avidity by direct measurement of HLA-A2/Mage3 complex density using a high-affinity TCR like monoclonal antibody. *Eur. J. Immunol.* 2005;35(10):2864–75.
17. Wittman VP et al. Antibody targeting to a class I MHC-peptide epitope promotes tumor cell death. *J. Immunol.* 2006;177(6):4187–95.
18. Neethling FA et al. Assessing vaccine potency using TCRmimic antibodies. *Vaccine* 2008;26(25):3092–102.
19. Weidanz JA et al. Levels of specific peptide-HLA class I complex predicts tumor cell susceptibility to CTL killing. *J. Immunol.* 2006;177(8):5088–97.
20. Klechevsky E et al. Antitumor activity of immunotoxins with T-cell receptor-like specificity against human melanoma xenografts. *Cancer Res.* 2008;68(15):6360–7.
21. Epel M et al. Targeting TARP, a novel breast and prostate tumor-associated antigen, with T cell receptor-like human recombinant antibodies. *Eur. J. Immunol.* 2008;38(6):1706–20.
22. Li D et al. Development of a T-cell Receptor Mimic Antibody against Wild-Type p53 for Cancer Immunotherapy. *Cancer Res.* 2017;77(10):2699–2711.
23. Li D et al. Engineering chimeric human and mouse major histocompatibility complex (MHC) class I tetramers for the production of T-cell receptor (TCR) mimic antibodies *PLoS One* 2017;12(4):e0176642.
24. Li D et al. Engineering chimeric human and mouse major histocompatibility complex (MHC) class I tetramers for the production of T-cell receptor (TCR) mimic antibodies. *PLoS One* 2017;12(4):e0176642.
25. Michaeli Y et al. Expression hierarchy of T cell epitopes from melanoma differentiation antigens: unexpected high level presentation of tyrosinase-HLA-A2 Complexes revealed by peptide-specific, MHC-restricted, TCR-like antibodies. *J. Immunol.* 2009;182(10):6328–41.
26. Verma B et al. Direct discovery and validation of a peptide/MHC epitope expressed in primary human breast cancer cells using a TCRm monoclonal antibody with profound antitumor properties. *Cancer Immunol. Immunother.* 2010;59(4):563–73.
27. Hawkins O et al. An HLA-presented fragment of macrophage migration inhibitory factor is a therapeutic target for invasive breast cancer. *J. Immunol.* 2011;186(11):6607–16.
28. Sergeeva A et al. An anti-PR1/HLA-A2 T-cell receptor-like antibody mediates complement-dependent cytotoxicity against acute myeloid leukemia progenitor cells. *Blood* 2011;117(16):4262–72.
29. Inaguma Y et al. Construction and molecular characterization of a T-cell receptor-like antibody and CAR-T cells specific for minor histocompatibility antigen HA-1H *Gene Ther.* 2014;21(6):575–584.

Structure	HID[a] Tautomerisation State
$\alpha_{58}\beta6_1$ TCR	Chain A: 3, 70, 74, 93, 114, 145, 260. Chain E: 151.
3M4E5 Fab	Chain A: 3, 70, 74, 93, 114, 145, 260. Chain D: 51.
MAG-IC3 TCR	Chain A: 3, 70, 93, 260. Chain E: 153.
Hyb3.3 Fab	Chain A: 3, 70, 93, 260. Chain D: 172, 212. Chain E: 95B , 189.
$\alpha_7\beta_2$ TCR	Chain A: 3, 70, 74, 93, 114. Chain B: 51. Chain D: 77. Chain E: 208.
ESK-1 Fab	Chain A: 3, 70, 93, 114. Chain D: 192.
NYBR1 TCR	Chain A: 3, 70, 74, 93, 151, 260. Chain E: 158.

Supplemental Table 2. Histidine tautomerisation state assignments for all MD simulations.
[a]HID corresponds to a histidine residue which is singly protonated on its Nδ1 nitrogen, with all other histidine residues simulated as singly protonated on their Nε2 nitrogen.